An Effective Consistency Correction and Blending Method for Camera-array-based Microscopy Imaging

Jiakun Bao[1, 2], Jingtao Fan[1, 2, *], Xiaowei Hu[3], Jinnan Wang[3], Lei Wang[1, 2]
[1]Department of Automation, Tsinghua University, Beijing, 100084, China
[2]Beijing Key Laboratory of Multi-dimension & Multi-scale Computational Photography (MMCP), Tsinghua University, Beijing, 100084, China
[3]Department of Electronic Engineering, Tsinghua University, Beijing, 100084, China
[*]*fanjingtao@mail.tsinghua.edu.cn*

***Abstract* - Camera-array-based microscopy imaging is an effective scheme to satisfy the requirements of wide field of view, high spatial resolution and real-time imaging simultaneously. However, with the increasing number of cameras and expansion of field of view, the nonlinear camera response, vignetting of camera lens, ununiformity of illumination system, and the low overlapping ratio all lower the quality of microscopic image stitching and blending. In this paper, we propose an image consistency correction and blending method for 5×7 camera-array-based 0.17-gigapixel microscopic images. Firstly, we establish an image consistency correction model. Then, we obtain the response functions and compensation factors. Next, we restore captured images based on above model. Finally, we adopt an improved alpha-blending method to stitch and blend images of multiple fields of view. Experimental results show that our proposed method eliminates the inconsistency and seams among stitched images effectively.**

Keywords - ***Camera Array; Consistency Correction; Response Function; Vignetting Compensation; Illumination Compensation; Improved Alpha Blending***

I. INTRODUCTION

Microscopy is an important tool in bioscience research. It is urgently required to dynamically observe micron/submicron sample details in centimeter-level fields of view in neuro and tumor studies. However, by the limitations of optical design and image acquisition methods, traditional microscope space-bandwidth product is difficult to improve, restricting the bioscience development.

With the support of National Natural Science Foundation of China, Tsinghua University has developed the multi-dimension and multi-scale computational photography instrument. This camera array based microscopic imaging instrument has advantages in real-time wide-field-of-view and high-resolution imaging, compared with tile scan microscopy [1, 2] or Fourier psychographic microscopy [3, 4]. As shown in Fig.1(a), our instrument contains an array of 35 5.5-million-pixel sCOMS cameras with 3%--6% of overlapping ratios and specialized rectangular lens (shown in Fig.1(c)). The field of view is 1cm × 1cm with a resolution of 1um, and the panoramic image contains over 0.17 gigapixel. Fig.1(b) is a simplified illustration of the light path.

Due to increase of camera numbers, expansion of the illumination area and complicated lens structures, the image inconsistency also becomes more prominent. Traditional macroscopic image mosaic algorithms, such as pyramid blending [5], multi-band blending [6], gradient domain stitching [7, 8], optimal seam stitching [9, 10], etc., cannot be directly applied to our system. The main reason is that, without consistency correction of microscopic images, it is difficult to obtain an acceptable blending effect through these traditional algorithms. On the other hand, existing mosaic algorithms of microscopic images [11, 12] are mostly designed for tile scan microscopes, which are not suitable for our large-scale camera array system with specialized optical lens structure. As for vignetting compensation, traditional methods generally either do not take nonlinear camera response into account [13] or do not separate the influence of uneven illumination [14], resulting in model errors and loss of universality. For correcting nonuniform brightness, a gain compensation [6, 15] is often used by minimizing an error function determined by overlapping pixels. These approaches lose efficiency sharply when overlapping area ratio come to be lower than 10%.

After obtaining the homography [16] for each image and accomplishing the image consistency correction, it is necessary to select an appropriate fusion method to fuse images of different cameras into a panoramic image. Due to the huge number of data and real-time demand in microscopic observation, a fast and effective blending method needs to be adopted. The traditional alpha blending method [17] calculates the pixel values of overlapping areas with a weighted average method. As the form of the weight distribution function is fixed, the traditional alpha blending method is not suitable for all situations. In this paper, an improved alpha blending method is proposed, which has more flexible forms as well as high-speed and user-interactive properties. These optimal features guarantee that our method can better solve the problem of low overlappings ratio image fusion in the actual splicing. Experiments show that our improved method indeed performs well, even when the overlapping ratio is very low (3%).

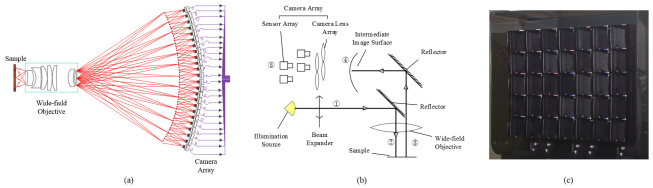

Figure 1. (a) Illusrtation of the array based microscope. (b) Simplified illustration of light path. (c) Camera lens array.

978-1-5090-6344-4/17/$31.00 ©2017 IEEE

II. IMAGE CONSISTENCY CORRECTION MODEL

A. Nonlinear Camera Response

The digital camera imaging process can be seen as a mapping from exposure to pixel value. As shown in Fig.2, this process begins when the scene light enters lens, after that the image sensor converts the photons incident during the exposure time into electrons to form an analog signal. Subsequently, the analog signal is formed into a voltage signal through the amplifier and then converted by the analog-to-digital converter into a digital signal. Finally, the digital signal is mapped to the pixel value.

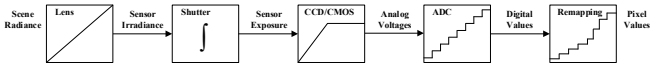

Figure 2. Image acquisition pipeline of digital camera.

The mapping from exposure value to pixel value can be explained as follows:

$$z = f(E\Delta t) \tag{1}$$

where z is the pixel value, E is the pixel-corresponding film irradiance value and Δt depicts the exposure time.

In order to avoid confusion，illuminance space refers to absolute or relative exposure value and grayscale space refers to pixel value. In the illuminance space, light is additive, so the compensation factor for illuminance does not change with the illuminance variation. In this way, the compensation factor obtained in the calibration environment is also applicable to the sample capturing environment.

B. Image Comsistency Correction Model

The image consistency correction model proposed in this paper can be describe as follow:

$$P'(x,y) = F\left(F^{-1}\left(Pix(x,y)\right)\cdot S_1\left(Centr_1(x,y)\right)\cdot S_2\left(Centr_2(x,y)\right)\right) \tag{2}$$

where $Pix'(x,y)$ is the corrected pixel value, $Pix(x,y)$ is the original pixel value, F (similar to f in Equation 1) maps relative exposure to pixel value, $S_1(Centr_1(x,y))$ is the vignetting compensation factor associated with the centrifugal distance of the single camera field, $S_2(Centr_2(x,y))$ is the illumination compensation factor correlated with the centrifugal distance of the whole camera array field.

The model can be understood as: the original pixel value is firstly transformed into the relative exposure value by the inverse F, and then multiplied by the vignetting compensation factor and the illumination compensation factor to obtain the ideal relative exposure. Finally, the ideal relative exposure is converted back into the ideal pixel value through F.

III. CALIBRATING THE CORRECTION MODEL PARAMETERS

A. Obtaining F through Exposure Stack Images

Obtaining the camera response function is generally based on the algorithm proposed by Debevec et al [18], which reduces the quadratic optimization problem to a linear least squares problem, then robustly solve the acquired overdetermined linear equation system using the singular value decomposition (SVD) method. In many cases, it is assumed that the pixel value of a point directly reflects the scene radiance [18]. However, the camera-array-based microscope to be calibrated in this paper has complex and unknown vignetting and illumination conditions. If we use the straightforward random sampling, the effect of vignetting and illumination unevenness will be introduced upon calculating the camera response function. In order to eliminate such influence, we use an exposure stack with enough exposure conditions to fit the function F, whose abscissa is the relative exposure value and ordinate is the corresponding pixel value.

In the experiment of measuring F, the observed object needs to have a smooth surface with uniform reflectivity, such as a silver coated mirror. The exposure time varies from microseconds to seconds. Due to the existence of vignetting, uneven illumination and other factors, the image is not uniform in grayscale (as shown in Fig.3(a)). Therefore, only the center area of the image is selected (can be considered to be without vignetting), and the pixel values of the selected region are averaged to eliminate the impact of uneven illumination. In this way, each image captured under a specific exposure time only provides a pair of "relative exposure value (h) -- pixel value (z)". The relative exposure $h = H / H_{normal}$, where $H = E\Delta t$ is the absolute exposure, and H_{normal} is the absolute exposure value corresponding to the pixel value $z = 128$. For most camera sensors, the mathematical model of the function F can be fitted with a polynomial function (as shown in Fig.3(b)). With the method described above, we acquire the response function for each camera of the array.

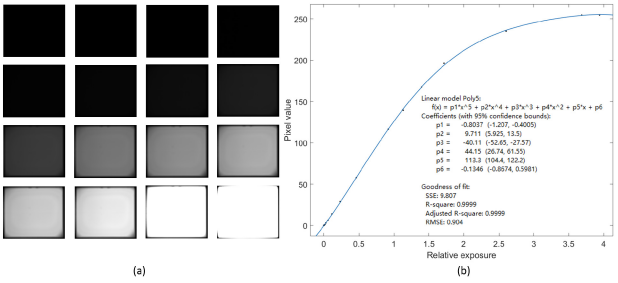

Figure 3. (a) Exposure stack. (b) Response function F.

B. Obtaining Vignetting Compensation Factors

When calibrating the vignetting compensation factor, it is necessary to turn off the microscopy illumination source. In this case, the observed object is a standard area light source without influence of the uneven illumination. We use the image of it as a template, and consider the average pixel value of the center area to be the ideal value.

The procedure of calibrating the vignetting compensation factors is as follows:

- Step1 We acquire the overexposed image for each camera in the array and each image is binarized to

978-1-5090-6344-4/17/$31.00 ©2017 IEEE

form a *Mask* . As the imaging area is smaller than the sensor area, the 1 values in the mask belong to the imaging area, and the 0 values belong to the area without imaging.

- Step2 Turn off the illumination source and observe a standard area light. We obtain several images under the same exposure time for each camera with neither overexposure nor underexposure.
- Step3 Images for each camera are averaged and median filtered for time and space smoothing. Then they are multiplied by the corresponding *Mask* to obtain the masked vignetting template (*MaskedVT*).
- Step4 Calculate the pixel-by-pixel vignetting compensation factors by the use of *MaskedVT* . The vignetting compensation factor (*VCF*) is calculated as:

$$VCF(x,y)=\frac{F^{-1}\left(\bar{z}\right)}{F^{-1}(MaskedVT(x,y))} \tag{3}$$

where $\bar{z}$ is the average pixel value of the center area of *MaskedVT* .

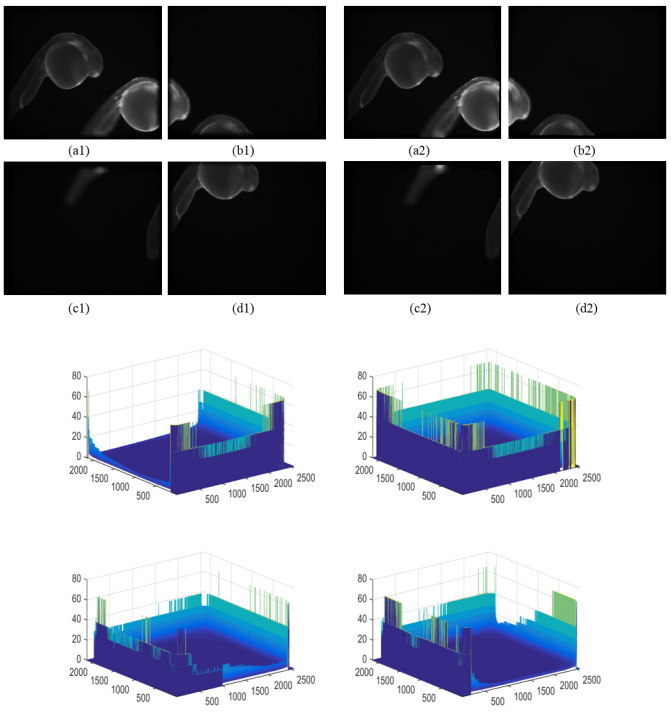

Figure 4. Fluorescence microscopic images of zebrafishes (a1)--(d1) before vignetting compensation; (a2)--(d2) after vignetting compensation; (e) compensation factors for fluorescence images.

For self-luminous fluorescent samples, only the vignetting compensation is required. According to Equation 2, the discrete correction formula can be exactly written as follows:

$$Pix'(x,y)=F\left(F^{-1}\left(Pix(x,y)\right)\cdot VCF(x,y)\right) \tag{4}$$

In the experiment, we compensate the fluorescence images of zebrafishes according to Equation 4, and the effects of compensation are demonstrated in Fig.4. It can be seen that before the compensation, the pixel values near the image edges attenuate quickly, resulting in information loss. After the compensation, the vignetting is significantly corrected, and the missing information is restored.

C. *Obtaining Illumination Compensation Factors*

When it comes to bright-field samples, we need to correct not only vignetting, but also overall illumination unevenness.

The procedure of calibrating the illumination compensation factors is as follows:

- Step1 Turn on the illumination source and observe a silver coated mirror. We take several images under the same exposure time for each camera without over or underexposure.
- Step2 The masked illumination template (*MaskedIT*) is obtained, similar to *MaskedVTI* .
- Step3 The illumination compensation factor (*ICF*) is calculated as:

$$ICF(x,y)=\frac{F^{-1}(\bar{z})}{F^{-1}(MaskedIT(x,y))\cdot VCF(x,y)} \tag{5}$$

where $\bar{z}$ is the averaged pixel value of the center area of *MaskedVTI* .

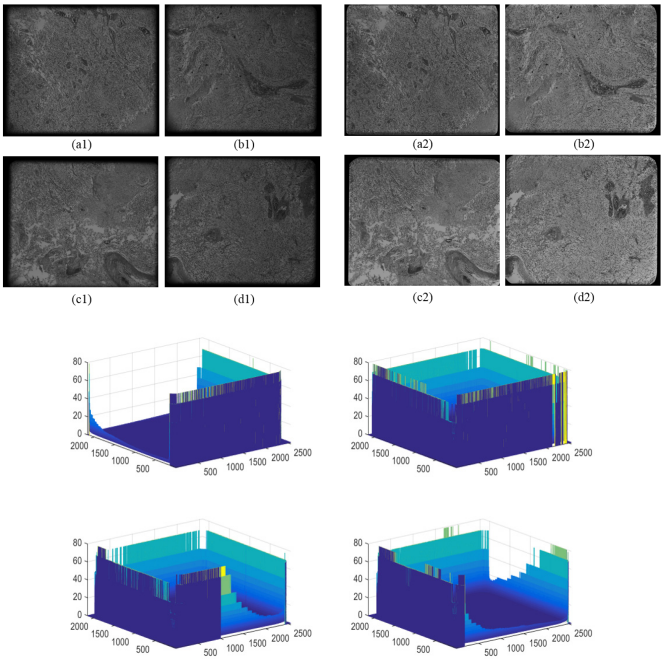

Figure 5. Bright-field microscopic images of glioma (a1)--(d1) before vignetting and illumination compensation; (a2)--(d2) after vignetting and illumination compensation; (e) compensation factors for bright-field images.

For bright-field samples, both vignetting and illumination compensations are required. The discrete form of the correction formula can be further written as:

$$Pix'(x,y)=F\left(F^{-1}\left(Pix(x,y)\right)\cdot VCF(x,y)\cdot ICF(x,y)\right) \tag{6}$$

In the experiment, we compensate the bright-field images of glioma according to Equation 6, and the effects are exhibited in Fig.5. It can be observed that before the compensation, on the one hand the pixel values near the image edges attenuate quickly due to vignetting, on the other hand the brightness of different cameras differs from each other due to illumination unevenness. After the compensation, both the vignetting and the illumination unevenness are significantly corrected, and the missing information is restored. In Fig.8, the illumination compensation effect can be seen more obviously.

IV. IMAGE BLENDDING METHOD

A. Traditional alpha Blending

Alpha blending fuses adjacent images in a weighted average manner, with the weight depending on the distance between the target pixel and the boundary of the overlapping region. In the case of two images, the pixel values after blending can be expressed as Equation 7.

$$I(x,y)=\begin{cases} I_1(x,y) & (x,y)\in I_1-I_1\cap I_2 \\ \omega_1 I_1(x,y)+\omega_2 I_2(x,y) & (x,y)\in I_1\cap I_2 \\ I_2(x,y) & (x,y)\in I_2-I_1\cap I_2 \end{cases} \tag{7}$$

In the situation where the left side of I_1 is stitched to the right side of I_2, we assume that $\hat{x}$ represents the distance from the pixel to be blended in the left-hand (right-hand) image to the right (left) border of the overlapping area, and *width* denotes the overlapping width. The linear weight distribution function can be written as:

$$\omega_i(\hat{x})=\left(\frac{\hat{x}}{width_i}\right),\quad \omega_i(\hat{y})=\left(\frac{\hat{y}}{height_i}\right) \tag{8}$$

When it comes to the situation where the up side of I_1 is stitched to down side of I_2, we get a quite similar distribution function.

B. Improved Alpha Blending

The traditional alpha-blending algorithm has some effect on eliminating the seam between stitched images, whereas it does not work for all kinds of situations, because the form of weight distribution function is fixed while image characteristics are variable. Therefore, we propose an improved alpha-blending algorithm, which preserves distance-dependent features, but adds more variable parameters, including power n, mid-value p and gamma γ. The left-to-right weight distribution function of the improved alpha blending can be written as:

$$\omega_i(\hat{x})=\begin{cases} [p(\frac{2\hat{x}}{width_i})^n]^{\frac{1}{\gamma}}, & \hat{x}\le\frac{width_i}{2} \\ \{1-(1-p)[2(1-\frac{\hat{x}}{width_i})]^n\}^{\frac{1}{\gamma}}, & \hat{x}>\frac{width_i}{2} \end{cases} \tag{9}$$

The up-to-down weight distribution function is quite similar:

$$\omega_i(\hat{y})=\begin{cases} [p(\frac{2\hat{y}}{width_i})^n]^{\frac{1}{\gamma}}, & \hat{y}\le\frac{width_i}{2} \\ \{1-(1-p)[2(1-\frac{\hat{y}}{width_i})]^n\}^{\frac{1}{\gamma}}, & \hat{y}>\frac{width_i}{2} \end{cases} \tag{10}$$

If we set $n=1$, $p=0.5$, and $\gamma=1$, Equation 9 and 10 are equal to Equation 8.

The three columns of Fig.6 respectively show the influence of power, mid-value, and gamma on the weight distribution function. With the increase of power, the distribution function tends to be increasingly flat near both ends and steeper in the central section. Thus, when power increases, large weights become larger, while small weights become smaller, that is, the pixel values of the overlapping area are more significantly determined by the pixels closer to the original image center. With the increase of mid-value or gamma, the sum value of the two weight distribution functions also increases. Besides, the sum near the central section increases more obviously. In other words, the brightness of the overlapping area increases more greatly near the center of the overlapping area than near the edges.

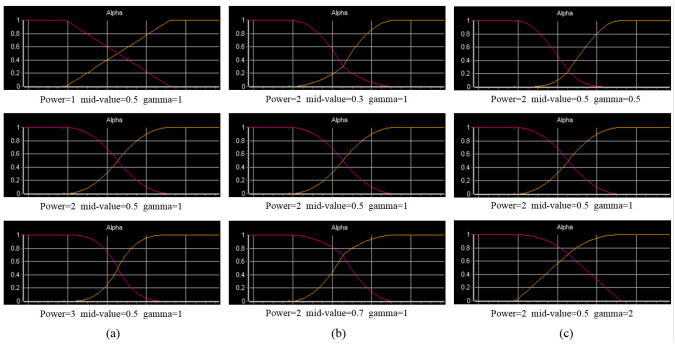

Figure 6. Weight distribution functions of improved alpha blending (a) influence of power; (b) influence of mid-value; (c) influence of gamma.

C. Results of Image Stitching and Blending

We register the 3D geometric relationship among cameras as homography matrixes by spatiotemporal encoding algorithm. Fig.7 and Fig.8 show the panoramic microscopic images after consistency correction and improved alpha blending. Fig.7 shows the panoramic fluorescence image of zebrafishes as well as its local enlarged image. In the absence of consistency compensation (Fig.7(a1, a2)), there are apparent seams in the overlapping area of the mosaic image and the information loss is serious. Using traditional alpha blending to stitch the images with consistency correction (Fig.7(b1, b2)), the information of the overlapping area is restored, but seams are still visible. Using improved alpha blending to stitch the images with consistency correction (Fig.7(c1, c2)), not only the information of the overlapping area is restored, but also the seams become invisible.

Fig.8 shows the panoramic bright-field image of glioma and its local amplification. Without consistency compensation (Fig.8(a1, a2)), there are significant visible seams in the overlapping area, meanwhile the information loss and

978-1-5090-6344-4/17/$31.00 ©2017 IEEE

brightness unevenness are both serious. Using traditional alpha blending to stitch the images after consistency correction (Fig.8(b1, b2)), the information the overlapping area is restored and the brightness unevenness is significantly improved, but seams are still visible. Relatively, using improved alpha blending to stitch the corrected images (Fig.8(c1, c2)), there are no information loss, visible seams, or brightness unevenness any more.

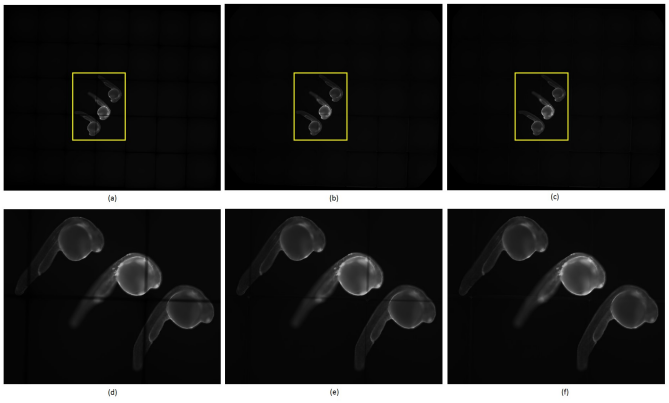

Figure 7. Panoramic fluorescence microscopic images of zebrafishes (a) blended without compensation; (b) vignetting compensation & traditional alpha blending; (c) vignetting compensation & improved alpha blending; (d) local enlarged image of (a); (e) local enlarged image of (b); (f) local enlarged image of (b).

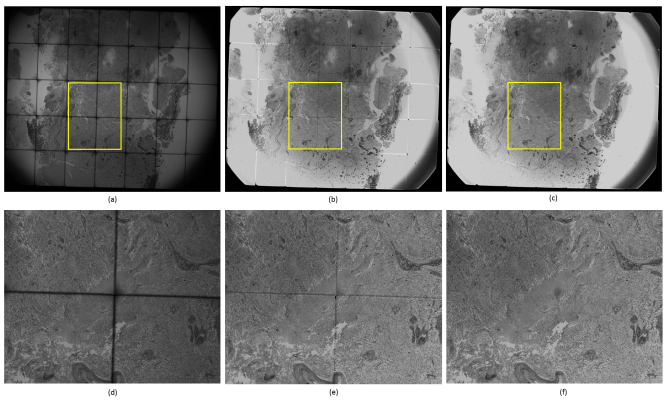

Figure 8. Panoramic bright-field microscopic images of glioma (a) blended without compensation; (b) vignetting and illumination compensation & traditional alpha blending; (c) vignetting and illumination compensation & improved alpha blending; (d) local enlarged image of (a); (e) local enlarged image of (b); (f) local enlarged image of (b).

V. CONCLUSION

Concerning the distinctive inconsistency of camera-array-based microscope images, we firstly analyze the limitations of existing methods. Based on factors resulting in inconsistency, we establish a consistency correction model including response function, vignetting compensation factor and illumination compensation factor. As the correction model does not depend on specific optical system structures, it has good generalizability. Then we experimentally calibrate the response function and compensation factors. After that, we perform the consistency correction on both fluorescence and bright field images and acquire remarkable results. Not only the missing information is restored, but also vignetting and brightness unevenness are eliminated. Finally, we use an improved alpha-blending method to obtain a panoramic image without any information loss, uneven brightness or visible seams. All experimental results show that our proposed method is more effective and robust compared with traditional methods. Moreover, our method can be used for reference by other camera-array-based microscopic imaging systems.

ACKNOWLEDGMENT

This work was supported by the Project of NSFC (No. 61327902 & 61671265).

REFERENCES

[1] Nan X, Potma E O, Xie X S. Nonperturbative chemical imaging of organelle transport in living cells with coherent anti-stokes Raman scattering microscopy[J]. Biophysical journal, 2006, 91(2): 728-735.

[2] Meyer T, Baumgartl M, Gottschall T, et al. A compact microscope setup for multimodal nonlinear imaging in clinics and its application to disease diagnostics[J]. Analyst, 2013, 138(14): 4048-4057.

[3] Zheng G, Horstmeyer R, Yang C. Wide-field, high-resolution Fourier ptychographic microscopy[J]. Nature photonics, 2013, 7(9): 739-745.

[4] Tian L, Liu Z, Yeh L H, et al. Computational illumination for high-speed in vitro Fourier ptychographic microscopy[J]. Optica, 2015, 2(10): 904-911..

[5] Adelson E H, Anderson C H, Bergen J R, et al. Pyramid methods in image processing[J]. RCA engineer, 1984, 29(6): 33-41.

[6] Brown M, Lowe D G. Automatic panoramic image stitching using invariant features[J]. International journal of computer vision, 2007, 74(1): 59-73.

[7] Pérez P, Gangnet M, Blake A. Poisson image editing[C]//ACM Transactions on Graphics (TOG). ACM, 2003, 22(3): 313-318.

[8] Levin A, Zomet A, Peleg S, et al. Seamless image stitching in the gradient domain[C]//European Conference on Computer Vision. Springer Berlin Heidelberg, 2004: 377-389.

[9] Milgram D L. Computer methods for creating photomosaics[J]. IEEE Transactions on Computers, 1975, 100(11): 1113-1119.

[10] Efros A A, Freeman W T. Image quilting for texture synthesis and transfer[C]//Proceedings of the 28th annual conference on Computer graphics and interactive techniques. ACM, 2001: 341-346.

[11] HSU W Y, POON W F, SUN Y N. Automatic seamless mosaicing of microscopic images: enhancing appearance with colour degradation compensation and wavelet - based blending[J]. Journal of Microscopy, 2008, 231(3): 408-418.

[12] Legesse F B, Chernavskaia O, Heuke S, et al. Seamless stitching of tile scan microscope images[J]. Journal of microscopy, 2015, 258(3): 223-232.

[13] Yu W. Practical anti-vignetting methods for digital cameras[J]. IEEE Transactions on Consumer Electronics, 2004, 50(4): 975-983.

[14] Kim S J, Pollefeys M. Robust radiometric calibration and vignetting correction[J]. IEEE transactions on pattern analysis and machine intelligence, 2008, 30(4): 562-576.

[15] Faas F G A, Avramut M C, van den Berg B M, et al. Virtual nanoscopy: generation of ultra-large high resolution electron microscopy maps[J]. J Cell Biol, 2012, 198(3): 457-469.

[16] Hartley R, Zisserman A. Multiple view geometry in computer vision[M]. Cambridge university press, 2003.

[17] Uyttendaele M, Eden A, Skeliski R. Eliminating ghosting and exposure artifacts in image mosaics[C]//Computer Vision and Pattern Recognition, 2001. CVPR 2001. Proceedings of the 2001 IEEE Computer Society Conference on. IEEE, 2001, 2: II-II.

[18] Debevec P E, Malik J. Recovering high dynamic range radiance maps from photographs[C]//ACM SIGGRAPH 2008 classes. ACM, 2008: 31